Local Conformational Changes in the Catalytic Core of the Trans-Acting Hepatitis Delta Virus Ribozyme Accompany Catalysis†

Dinari A. Harris, David Rueda, and Nils G. Walter*

Department of Chemistry, The University of Michigan, 930 North University, Ann Arbor, Michigan 48109-1055

Received May 8, 2002; Revised Manuscript Received August 15, 2002

ABSTRACT: The hepatitis delta virus (HDV) is a human pathogen and satellite RNA of the hepatitis B virus. It utilizes a self-cleaving catalytic RNA motif to process multimeric intermediates in the double-rolling circle replication of its genome. Previous kinetic analyses have suggested that a particular cytosine residue (C_{75}) with a pK_a close to neutrality acts as a general acid or base in cleavage chemistry. The crystal structure of the product form of a cis-acting HDV ribozyme shows this residue positioned close to the 5′-OH leaving group of the reaction by a trefoil turn in the RNA backbone. By modifying G_{76} of the trefoil turn of a synthetic trans-cleaving HDV ribozyme to the fluorescent 2-aminopurine (AP), we can directly monitor local conformational changes in the catalytic core. In the ribozyme−substrate complex (precursor), AP fluorescence is strongly quenched, suggesting that AP_{76} is stacked with other bases and that the trefoil turn is not formed. In contrast, formation of the product complex upon substrate cleavage or direct product binding results in a significant increase in fluorescence, consistent with AP_{76} becoming unstacked and solvent-exposed as evidenced in the trefoil turn. Using AP fluorescence and fluorescence resonance energy transfer (FRET) in concert, we demonstrate that this local conformational change in the trefoil turn is kinetically coincidental with a previously observed global structural change of the ribozyme. Our data show that, at least in the trans-acting HDV ribozyme, C_{75} becomes positioned for reaction chemistry only along the trajectory from precursor to product.

The hepatitis delta virus ribozyme is among a class of small endonucleolytic RNAs that catalyze a reversible self-cleavage reaction necessary for the replication and propagation of their satellite RNA genomes. Specifically, the hepatitis delta virus ribozyme is a unique RNA motif found in the human hepatitis delta virus (HDV)[1] (*1*). HDV is a satellite of the hepatitis B virus (HBV); coinfection of HDV and HBV results in intensification of the disease symptoms associated with the hepatitis B virus (*2*). The small RNA genome of HDV replicates through a double-rolling circle mechanism, whereby multimeric units of genomic and antigenomic RNA strands are produced, followed by self-cleavage and ligation into circular monomers (*1*, *3*). Self-cleavage activity in the genomic and antigenomic RNAs resides within continuous 85-nucleotide sequences that both form a nearly identical secondary structure consisting of a nested double pseudoknot (*4*, *5*).

The genomic and antigenomic forms of the HDV ribozyme catalyze self-cleavage by a transesterification reaction, which requires deprotonation of the adjacent 2′-OH group and its nucleophilic attack on the scissile phosphate, resulting in formation of 2′,3′-cyclic phosphate and 5′-OH termini (*5*). The reaction mechanism of the HDV ribozyme has been extensively studied. The crystal structure of the self-cleaved genomic ribozyme reveals that the base cytosine 75 (C_{75}) is situated in the active site cleft and, thus, in the proximity of the 5′-OH leaving group (Figure 1a,b). Therefore, C_{75} in the genomic ribozyme has been proposed to participate directly in reaction chemistry as either a general acid or general base catalyst (*6*).

Several biochemical and mutagenesis studies support the idea that C_{75} in the genomic ribozyme and the corresponding αC_{76} (α used to distinguish antigenomic numbering) in the antigenomic ribozyme are involved in catalysis (*7*−*10*). The pH dependence of self-cleavage (or cis cleavage) by the HDV ribozyme reveals a macroscopic apparent pK_a that approaches neutrality. In a widely accepted model, this pK_a reflects the ionization equilibrium of N3 in C_{75} which therefore is strongly shifted in the folded ribozyme compared to that in the free base (p$K_a \approx 4.2$). A decrease in this pK_a for self-cleavage of an antigenomic ribozyme with an $\alpha C_{76}A$ mutation was observed, consistent with A substituting for C in this position to act as a general base catalyst (*8*). However, the pH profile of the genomic ribozyme in the presence of 1 M NaCl and 1−100 mM EDTA favors a model where C_{75} acts as a general acid during catalysis (*9*, *11*). This latter mechanism is in agreement with the crystal structure of the self-cleaved genomic ribozyme, which shows N3 of C_{75} within hydrogen bonding distance of the 5′-OH leaving group. In addition, C_{75} is hydrogen bonded to the phosphate group of C_{22}, increasing the local electron density and providing a mechanism for a shift in pK_a, such that it is

† This work was supported by NIH Grant GM62357 to N.G.W., a Rackham Merit predoctoral fellowship and NIH Molecular Biophysics Training Grant to D.A.H., and a postdoctoral fellowship from the Swiss National Fonds to D.R.

* To whom correspondence should be addressed. Phone: (734) 615-2060. Fax: (734) 647-4865. E-mail: nwalter@umich.edu.

[1] Abbreviations: AP, 2-aminopurine; FRET, fluorescence resonance energy transfer; fwhm, full width at half-maximum; HDV, hepatitis delta virus.

10.1021/bi026101m CCC: $22.00
Published on Web 09/14/2002

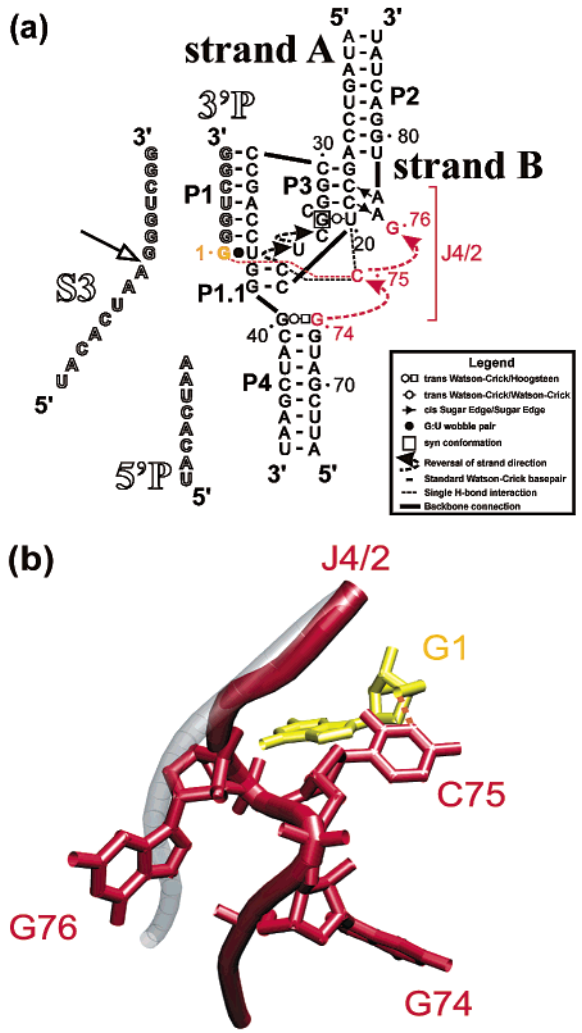

FIGURE 1: Sequence and structure of the HDV ribozyme. (a) Two-dimensional representation of our synthetic trans-acting HDV ribozyme construct D1. The ribozyme−3′-product complex is shown annotated according to ref *66* with the tertiary structure of the postcleavage crystal structure which it models (*6*). The colored nucleotides are the ones shown in detail in panel b. The ribozyme portion consists of two separate RNA strands (A and B). Substrate strand S3 (outlined) is cleaved at the arrow into the 5′- and 3′-products (5′P and 3′P, respectively), and 5′P dissociates from the ribozyme−3′-product complex. (b) Trefoil turn in J4/2 as observed in the postcleavage crystal structure (red). C_{75} is positioned deep in the catalytic core making a single hydrogen bond (orange) with the 5′-hydroxyl leaving group of G_1 (yellow), whereas G_{76} loops out exposing it to solvent. Also shown as an overlay (gray) is the more regular backbone trajectory between G_{76} and U_{79}. This figure was generated using VMD 1.7.2 and Pov-Ray 3.1g for Windows.

protonated around neutral pH (*6*). Thus, C_{75} is in a position in which it may donate a proton to relieve the developing charge on the leaving 5′-oxyanion group in the reaction transition state (*6*). Recently, nucleotide analogue interference mapping (NAIM) of the genomic ribozyme has provided further evidence for the importance of the ionization of C_{75} in the cis cleavage reaction, as it is the only cytidine residue that must be protonated for ribozyme activity (*10*).

The use of an RNA base to facilitate transition-state chemistry appears to be surprisingly common among RNA catalysts. For example, biochemical and structural studies suggest that the hairpin ribozyme may use two catalytically essential nucleotide residues, G_8 and A_{38}, to function as the proton acceptor and donor, respectively (*12*, *13*). An analogous proposal has been made for the large subunit of the ribosome, where no amino acid side chains or metal ions but rather a conserved adenosine (A_{2451} in *Escherichia coli* numbering) is found in sufficient proximity to potentially act as a catalyst in peptidyl transfer (*14*), although this is still controversial (*15*, *16*). These discoveries reveal that RNA bases in ribozymes can participate in catalysis in a manner similar to that of amino acid side chains in protein enzymes. Hence, the finding that the HDV ribozyme utilizes one of its RNA side chains in acid−base catalysis has led the way to fundamental insights into RNA catalysis.

Studies of the folding pathway of the HDV ribozyme are key to our understanding of how the RNA positions C_{75} in the active site cleft such that it becomes both chemically activated and poised for catalysis. The crystal structure of the self-cleaved genomic ribozyme gives hints about how this positioning occurs. C_{75} and its two adjacent nucleotides, G_{76} and G_{74}, form a "trefoil" turn that pushes C_{75} deeply into the catalytic core (Figure 1b) (*6*). In particular, extrusion of G_{76} allows for a backbone geometry that projects C_{75} toward the 5′-OH leaving group. With this in mind, we have devised a fluorescence-based technique for monitoring the unstacking of the nucleotide in position 76 as it extrudes from neighboring bases into solvent, by substituting 2-aminopurine (AP) for G_{76}. AP is a fluorescent guanine analogue that is highly sensitive to local stacking interactions with other bases and can be selectively excited in the presence of the natural bases (*17*). Mutagenesis studies suggest that the chosen substitution site can be mutated with only a modest loss of activity (*7*). When monitoring conformational changes at position 76 through AP fluorescence in the trans-acting HDV ribozyme, we observe a substantial local conformational change that accompanies ribozyme catalysis. Our results complement a previous study in which we found, using fluorescence resonance energy transfer (FRET), that a significant global conformational change concurs with catalysis (*18*). Using AP fluorescence and FRET in concert, we demonstrate here that the global structural change upon cleavage is coupled to, and probably the consequence of, local conformational rearrangements in and around the catalytic core that lead to proper positioning of C_{75}.

MATERIALS AND METHODS

Preparation of RNA Oligonucleotides. All RNA oligonucleotides were obtained commercially from Dharmacon Research, Inc., with 2′-protection groups (*19*) and were deprotected following the manufacturer's recommendations. Deprotected RNA was purified by denaturing 20% polyacrylamide, 8 M urea, gel electrophoresis, diffusion elution into 0.5 M NH_4OAc, 0.1% SDS, and 0.1 mM EDTA overnight at 4 °C, chloroform extraction, and ethanol precipitation, followed by C_8 reverse-phase HPLC with a linear acetonitrile elution gradient in triethylammonium acetate, as described previously (*20*). The noncleavable substrate analogue was modified with a 2′-methoxy group at the cleavage site (Figure 1a). The 3′-product had the sequence 5′-GGGUCGG-3′. RNA concentrations were calculated from the absorbance at 260 nm after background correction. 5′-Fluorescein was incorporated into the RNA during synthesis by Dharmacon Research, Inc., while tetramethylrhodamine was postsynthetically attached to a 3′-amino linker as previously described (*18*). The concentrations

of fluorescein- and tetramethylrhodamine-labeled RNAs were corrected for the additional absorbance of the fluorophores by using the relations $A_{260}/A_{492} = 0.3$ and $A_{260}/A_{554} = 0.49$, respectively.

Cleavage Reactions. Activities of ribozymes with G_{76} modifications were determined using the three-strand HDV ribozyme construct depicted in Figure 1a. All cleavage reactions were conducted under single-turnover (pre-steady-state) conditions and using standard conditions of 40 mM Tris-HCl (pH 7.5) and 11 mM $MgCl_2$, at 37 °C, unless otherwise stated. The ribozyme was prepared by preannealing strand A and twice the concentration of strand B in standard buffer, heating to 70 °C for 2 min, and cooling to room temperature. After preincubation at 37 °C for 15 min, a trace amount (<4 nM) of 5′-^{32}P-labeled substrate (also in standard buffer) was added to a saturating concentration of 400 nM ribozyme (based on the strand A concentration), unless otherwise noted. Aliquots (5 μL) were taken at the appropriate time intervals, and the reaction was quenched with 10 μL of 80% formamide, 0.025% xylene cyanol, 0.025% bromophenol blue, and 50 mM EDTA. The 5′-cleavage product was separated from the uncleaved substrate by denaturing 20% polyacrylamide, 8 M urea, gel electrophoresis, and was quantified and normalized to the sum of the substrate and product bands using a PhosphorImager Storm 840 instrument with ImageQuant software (Molecular Dynamics). Time traces of product formation were fit to the single-exponential first-order rate equation $y = y_0 + A_1(1 - e^{-t/\tau_1})$, employing Marquardt−Levenberg nonlinear least-squares regression (Microcal Origin 6.0), where A_1 is the amplitude and $1/\tau_1$ the pseudo-first-order rate constant k_{obs}. Ribozyme (Rz) and magnesium ion (Mg^{2+}) dependencies of this rate constant were fit to the binding equations:

$$k_{obs} = k_{cleav}\frac{[Rz]^n}{[Rz]^n + K_M{}^n}$$

and

$$k_{obs} = k_{max}\frac{[Mg^{2+}]^n}{[Mg^{2+}]^n + Mg_{1/2}{}^n}$$

to yield the cleavage rate constant k_{cleav} under standard conditions, the apparent ribozyme and magnesium dissociation constants K_M and $Mg_{1/2}$, respectively, and a cooperativity coefficient n (*21*). For the pH dependence, cleavage was assayed in a buffer with 25 mM MES, 25 mM acetic acid, and 50 mM Tris (pH 4.0−8.0) or a buffer with 50 mM MES, 25 mM Tris, and 25 mM 2-amino-2-methyl-1-propanol (pH 8.5−9.5) (*8*). The pH-dependent rate constants were fit to the following equation (*22*)

$$k_{obs} = k_{max}/(1 + 10^{pK_{a1}-pH} + 10^{pH-pK_{a2}})$$

Steady-State Fluorescence Measurements. Steady-state fluorescence spectra and intensities were recorded on an Aminco-Bowman Series 2 (AB2) spectrofluorometer (Thermo Spectronic). For the HDV ribozyme substituted with only AP, steady-state measurements were performed in a manner similar to previously described procedures (*23*, *24*). Specifically, the annealed ribozyme (final concentration of 200 nM; with a minimum of a 2-fold excess of unlabeled strand A) was incubated at 37 °C for at least 15 min in standard buffer and then transferred to a 150 μL cuvette. The substrate, noncleavable substrate analogue, or 3′-product was manually added at a (saturating) 5-fold excess, unless otherwise stated. For kinetic experiments, AP was excited at 300 nm (4 nm bandwidth) and fluorescence emission was monitored at 360 nm (8 nm bandwidth). The emission signal was normalized with its value immediately after formation of the ribozyme−substrate complex to obtain the relative AP fluorescence. The resulting time traces were fit similarly to the cleavage time courses, to single- or double-exponential increase and decrease functions of the form $y = y_0 + A_1(1 - e^{-t/\tau_1}) + ...$ and $y = y_0 + A_1e^{-t/\tau_1} + ...$, respectively, as required.

For the HDV ribozyme substituted with AP_{76} and labeled with fluorescein and tetramethylrhodamine, the protocol was the following. For AP fluorescence measurements, AP was excited at 300 nm (8 nm bandwidth) and fluorescence emission was recorded at 360 nm (8 nm bandwidth). For FRET measurements, the standard buffer was supplemented with 25 mM dithiothreitol as a radical quencher. Fluorescein was excited at 490 nm (4 nm bandwidth), and fluorescence emission was recorded simultaneously at the fluorescein (520 nm, 8 nm bandwidth) and tetramethylrhodamine (585 nm, 8 nm bandwidth) wavelengths, by shifting the emission monochromator back and forth. A FRET ratio Q ($=F_{585}/F_{520}$) was calculated and normalized with its starting value to obtain the relative FRET efficiency. The resulting time traces were fit to exponential functions as described above.

pH Titrations of HDV-AP_{76}. The fluorescence intensity of AP when substituted at position 76 was measured as a function of pH. Annealed ribozyme complexes (200 nM AP-substituted ribozyme strand B, 400 nM strand A, and 1000 nM substrate, noncleavable substrate analogue, or 3′-product) were incubated at 37 °C for at least 15 min in 11 mM $MgCl_2$, 25 mM MES, 25 mM acetic acid, and 50 mM Tris (pH 4.0−8.0) or 25 mM sodium citrate (pH 2.0−4.0). The pH was titrated with dilute HCl, and solutions were allowed to re-equilibrate for 3 min at 37 °C after each acid addition. The AP emission spectrum was measured between 320 and 500 nm (8 nm bandwidth) upon excitation at 290 nm (8 nm bandwidth). The peak intensity at 360 nm was recorded for all pH values. The fluorescence was corrected for volume changes from the addition of dilute HCl, and the pK_a value was determined by fitting the curves to the equation $F_{obs} = F_{max}/(1 + 10^{pK_a-pH})$ (*9*). The reported data are the result of three independent titrations. As a control, the fluorescence intensity of 2-aminopurine 2′-deoxyribose 5′-triphosphate (TriLink Biotechnologies) was measured.

Time-Resolved FRET Measurements. The global structure of the HDV ribozyme with AP substitution at position 76 was studied by trFRET analysis of ribozyme complexes doubly labeled with fluorescein and tetramethylrhodamine as previously described (*18*). Annealed ribozyme complexes (70 μL; 1 μM doubly labeled ribozyme strand B, 3 μM strand A, and 6 μM substrate, noncleavable substrate analogue, or 3′-product) were incubated at 37 °C for at least 15 min in standard buffer (supplemented with 25 mM DTT), prior to collecting time-resolved donor emission profiles using time-correlated single-photon counting, a process similar to previously described procedures (*25*). A frequency-doubled Nd:YVO_4 laser (Spectra-Physics Millenia Xs-P, operated at

9.0 W) pumped a frequency-doubled, mode-locked Ti: sapphire laser (Spectra-Physics Tsunami, operated at 1 W) that excited fluorescein at 490 nm by 2 ps width pulses, picked down to 4 MHz. Isotropic emission was detected at 520 nm (10 nm band-pass interference filter) in 4096 sampling channels, with a time increment of 12 ps/channel, up to >40000 peak counts, and under magic angle polarizer conditions. To measure donor−acceptor distances, two time-resolved fluorescence decays were collected, with and without the acceptor in place. The effect of the acceptor on the decay of fluorescein emission in the doubly labeled complex was then used to extract a three-dimensional Gaussian distance distribution between the two fluorophores as previously described in detail (*18*, *25*, *26*). To calculate a mean distance, a value of 55 Å for the Förster distance R_0 of fluorescein and tetramethylrhodamine was used (*25*), assuming a value of $^2/_3$ for the orientation factor as experimentally supported by low fluorophore anisotropies (*18*).

FRET Gel Shift Assays. FRET gel shift assays were conducted to test the homogeneity of the various ribozyme−substrate complexes, as previously described (*18*). Nondenaturing 10% polyacrylamide (19:1 acrylamide:bisacrylamide ratio) gels containing 40 mM Tris-HCl (pH 7.5) and 11 mM $Mg(OAc)_2$ were assembled with the electrophoresis unit and equilibrated to 4 °C for at least 2 h. Ten picomoles of doubly fluorophore-labeled ribozyme strand B was annealed to 20 pmol of strand A by heating for 2 min to 70 °C and cooling to room temperature in 40 mM Tris-HCl (pH 7.5), 11 mM $MgCl_2$, and 10% glycerol. The ribozyme was equilibrated at 37 °C for at least 15 min prior to addition of 50 pmol of substrate, noncleavable substrate analogue, or 3′-product (total volume of 20 μL). These samples were loaded on the gel, and an electric field of 5 V/cm was immediately applied. After electrophoresis for 24 h, the gel was scanned between its low-fluorescence glass plates in a FluorImager SI fluorescence scanner with ImageQuant software (Molecular Dynamics) as described previously (*18*, *27*). A laser excites fluorescein at 488 nm, and the gel is scanned for fluorescence emission using a photomultiplier tube with either a 530 nm band-pass (for the donor fluorescein) or a 610 nm long-pass filter (for the acceptor tetramethylrhodamine). RNAs labeled with only fluorescein and only tetramethylrhodamine were included as color calibration standards. From the volume reports, a measure of FRET efficiency of selected bands was calculated as $F_{acceptor}/F_{donor}$. With the readout of F_{donor} defined as being green and that of $F_{acceptor}$ as red, the corresponding color images were superimposed using Photoshop 5.5 (Adobe) to generate Figure 6.

RESULTS

A Base Substitution of G_{76} with AP Is Tolerated in a Trans-Acting HDV Ribozyme with an Only Modest Decrease in Catalytic Activity. The trans-cleaving HDV ribozyme used in this study, D1, is a synthetic three-strand construct, which consists of ribozyme strands A and B and substrate strand S3 (Figure 1a). Previously, we characterized in detail the catalytic activity of this trans-cleaving construct under a variety of conditions (*18*). Our data showed that this construct has cleavage rate constants as well as metal ion, temperature, and pH dependencies similar to those of other trans-acting HDV ribozymes. To evaluate the effect that a G_{76}AP

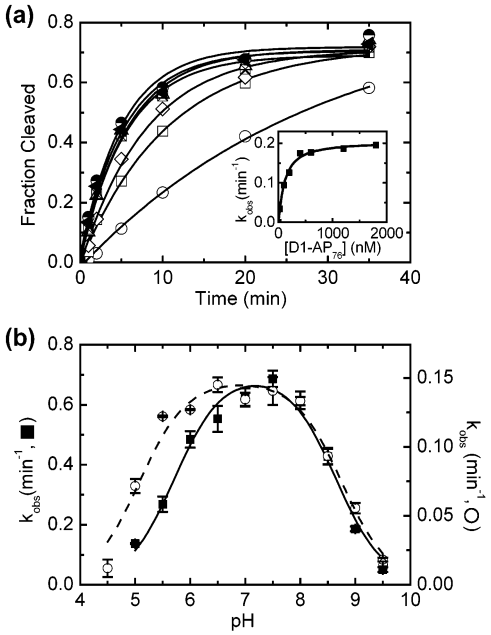

FIGURE 2: Cleavage of substrate strand S3 by HDV ribozyme construct D1-AP_{76} under single-turnover conditions. (a) Cleavage time courses of D1-AP_{76} under standard conditions of 40 mM Tris-HCl (pH 7.5) and 11 mM $MgCl_2$ at 37 °C, with varying ribozyme concentrations [(○) 50, (□) 100, (◇) 200, (△) 400, (crossed box) 800, (◓) 1200, and (tilted triangle) 1600 nM]. Data were fit to a single-exponential increase function (—) to yield the rate constants k_{obs} reported in the inset (total fraction cleaved, ~70%). In the inset, the dependence of k_{obs} on ribozyme concentration was fit to a binding equation (—) (see Materials and Methods), yielding a k_{cleav} of 0.20 min^{-1} (K_M = 114 nM). (b) pH dependence of the observed cleavage rate constants. The data were fit [see Materials and Methods; D1 (—■—) and D1-AP_{76} (- -○- -)] to yield the two pK_a values for each construct reported in Table 1.

mutation has on this construct, we measured its cleavage rate constants, as well as its metal ion and pH dependencies, and compared them to those of the D1 wild type with G_{76}.

First, we measured the cleavage rate constant under standard single-turnover (pre-steady-state) reaction conditions, which consisted of trace amounts of radiolabeled S3 substrate with a saturating excess of 400 nM ribozyme in 40 mM Tris-HCl (pH 7.5) and 11 mM $MgCl_2$ at 37 °C (see Materials and Methods). In addition, reactions were performed at ribozyme concentrations varying between 25 and 1800 nM to ensure reaching saturation. Figure 2a shows the resulting reaction time courses for the G_{76}AP mutant. The observed pseudo-first-order rate constants (k_{obs}) were plotted as a function of ribozyme concentration and fit to a simple binding equation (inset of Figure 2a; see Materials and Methods), yielding rate constants for the rate-limiting step of cleavage (k_{cleav}) at 37 °C of 1.34 and 0.20 min^{-1} for the D1 wild type and the G_{76}AP mutant, respectively (Table 1). The ~7-fold decrease in catalytic activity with the G_{76}AP mutation is on the same order of magnitude as that for other mutations, including G_{76} to adenine (A), inosine (I), uracil (U), or 4-thiouracil (SU) (Table 2). Cleavage rate constants followed this trend: wild type > G_{76}SU ≈ G_{76}I > G_{76}U > G_{76}AP ≈ G_{76}A. A moderate decrease in cleavage activity upon substitution of G_{76} is also consistent with previous mutagenesis studies, particularly in the cis-cleaving genomic HDV ribozyme where substituting G_{76} for U results in an ~15-fold decrease in catalytic activity (*7*).

Table 1: Cleavage Rate Constants, Metal Ion Dissociation Constants, and pK_as for HDV Ribozyme Construct D1 and Its G76AP Mutant[a]

parameter	D1−S3	D1-AP_{76}−S3
k_{cleav} (min^{-1}) (pH 7.5, 11 mM Mg^{2+}, 37 °C)	1.34 ± 0.07	0.20 ± 0.01
$Mg_{1/2}$ (mM)	9 ± 1	17 ± 3
pK_{a1}, pK_{a2}	5.7, 8.6	5.1, 8.7
k_{on} (M^{-1} min^{-1})	ND	$(2.4 \pm 0.2) \times 10^6$
k_{off} (min^{-1})	ND	0.20 ± 0.04

[a] The single-turnover cleavage rate constant k_{cleav} was determined with substrate strand S3 and saturating ribozyme as described in the text (standard conditions, 40 mM Tris-HCl, pH 7.5, 11 mM $MgCl_2$, and 37 °C). $Mg_{1/2}$s were derived as described in Materials and Methods, pK_as from the data in Figure 2b, and k_{on} and k_{off} from the data in panels b and c of Figure 3, respectively. ND means not determined.

Table 2: Cleavage Activity of G_{76} Modifications on the HDV Ribozyme[a]

	k_{obs} (min^{-1})		k_{obs} (min^{-1})
wild type	0.84 ± 0.02	U	0.28 ± 0.04
SU	0.54 ± 0.02	AP	0.17 ± 0.01
I	0.53 ± 0.01	A	0.17 ± 0.01

[a] Observed rate constants (k_{obs}) were measured under standard conditions (single-turnover, 40 mM Tris-HCl, pH 7.5, 11 mM $MgCl_2$, 400 nM ribozyme, and 37 °C) for trans-cleaving HDV ribozyme construct D1 (Figure 1a); errors were estimated from at least three independent measurements.

Next, we compared Mg^{2+} binding affinities of the wild-type and G_{76}AP mutant D1 constructs. Cleavage activity was measured under standard single-turnover conditions (at 400 nM ribozyme excess) but at varying magnesium concentrations (2−200 mM Mg^{2+}). The observed rate constants for the G_{76} wild-type ribozyme increase substantially from 0.075 to 1.47 min^{-1} in this range, while the G_{76}AP mutant shows a more modest increase from 0.26 and 0.393 min^{-1}. The resultant magnesium titration midpoints ($Mg_{1/2}$) are 9 and 17 mM, respectively (Table 1). These Mg^{2+} affinities are somewhat lower than that reported for a cis-cleaving HDV ribozyme (1 mM) (*28*), but higher than that of another three-strand ribozyme construct (40 mM) (*29*).

Finally, we compared the pH dependence of cleavage of the wild type and the G_{76}AP mutant to verify that the latter utilizes a mechanism similar to that of the unmodified D1 construct. Such pH profiles have been critical in establishing the involvement of C_{75} in the catalytic mechanism of the HDV ribozyme. Figure 2b shows the resulting curves. Both constructs show bell-shaped pH profiles similar to those of previously characterized trans-acting (*22*) and cis-acting HDV ribozymes (*30*). From the pH dependence of the wild-type G_{76} D1 construct, two pK_as of 5.7 and 8.6 are derived, while the pK_as of the G_{76}AP mutant are 5.1 and 8.7 (Figure 2b and Table 1). It is noteworthy that both pH profiles suggest that a pH-dependent step is rate-limiting at low pH (*5*, *31*).

Steady-State 2-Aminopurine Fluorescence Assays Reveal Differences between Pre- and Postcleavage Structures and Report on the Folding Kinetics of the HDV Ribozyme. AP is a strongly fluorescent base (excitation maximum at 320 nm, emission maximum at 360 nm, quantum yield of 68%) and is highly sensitive to local stacking interactions with other bases. The fluorescence of AP is quenched when it stacks with other bases, but increases substantially when it becomes fully exposed to solvent (*32*−*34*). AP has recently been utilized as a fluorescent probe for local dynamics in other catalytic RNAs, such as the hammerhead and hairpin ribozymes (*12*, *23*, *24*). To observe localized structural changes in the catalytic core of the HDV ribozyme, we have monitored changes in AP steady-state fluorescence of our G_{76}AP modified D1 construct (D1-AP_{76}) upon addition of either substrate or product. In all fluorescence assays, saturating 2- and 5-fold excesses of the unmodified strand A and substrate (or product), respectively, were added under standard conditions (see Materials and Methods).

The fluorescence changes of AP_{76} indicate that a substantial conformational rearrangement around this position accompanies catalysis (Figure 3a). In particular, addition of saturating concentrations of a chemically blocked, noncleavable substrate analogue of S3 (ncS3) to the assembled ribozyme results in a slight (∼12%) decrease in relative AP fluorescence (inset of Figure 3a). This fluorescence quenching suggests that AP becomes more stacked as a result of formation of the ribozyme−substrate (precursor) complex. The pseudo-first-order rate constant for this decrease is linearly dependent on the excess concentration of ncS3, indicating that this fluorescence decrease is a direct result of substrate binding. On the basis of this linear dependence, we deduce a second-order substrate binding rate constant k_{on} of 2.4×10^6 M^{-1} min^{-1} (Figure 3b and Table 1), similar to a previously determined value for this ribozyme−substrate complex at 25 °C instead of 37 °C (*18*).

In contrast, when a saturating concentration of the cleavable substrate S3 is added, we observe an ∼7-fold increase in AP fluorescence (Figure 3a). The rate constant of 0.27 min^{-1} for this single-exponential increase is similar to the cleavage rate constant obtained in the standard autoradiographic assay (0.17 min^{-1}; see above). This suggests that the observed fluorescence increase is the result of substrate cleavage, which leads to rapid dissociation of its 5′-portion (*5*, *18*) and formation of the ribozyme−3′-product complex. Notably, initial binding of substrate, which is associated with a fluorescence decrease, results in a slight lag phase in the fluorescence increase (inset of Figure 3a).

Direct formation of the ribozyme−3′-product complex was initiated by adding a saturating excess of the 3′-product of the substrate (termed 3′P, sequence of 5′-GGGUCGG-3′) to the assembled ribozyme. Previously, it has been shown that the 3′-product remains bound to the ribozyme after cleavage, while the 5′-product rapidly dissociates (*4*, *18*). We find that addition of 3′P and formation of the ribozyme−3′P complex result in a fast (slightly double-exponential) ∼9.5-fold increase in the relative AP_{76} fluorescence. We estimate the rate constant for this fluorescence increase to be ∼7.1 min^{-1} at 1 μM 3′P. This substantial dequenching of its fluorescence implies that AP_{76} becomes significantly unstacked and exposed to solvent in the ribozyme−3′-product complex. This observation is consistent with the postcleavage crystal structure of the genomic form of the cis-cleaving HDV ribozyme, which shows G_{76} extruding into solvent (Figure 1b). Furthermore, the fluorescence increase following substrate cleavage is approximately 75% of that which occurs upon direct formation of the ribozyme−3′P complex, consistent with the 75% conversion of S3 into 3′P by the G_{76}-AP mutant under standard cleavage conditions (Figure 2a).

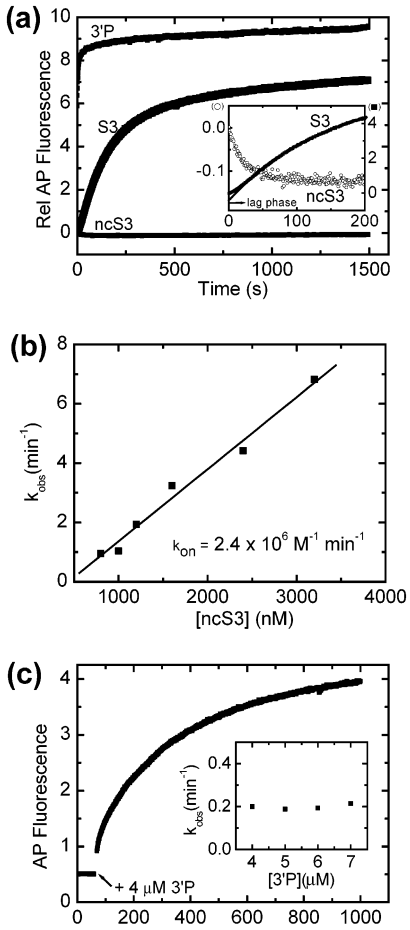

FIGURE 3: Steady-state 2-aminopurine fluorescence measurements using 200 nM ribozyme D1-AP_{76} in 40 mM Tris-HCl (pH 7.5) and 11 mM $MgCl_2$ at 37 °C. (a) Change over time in the relative AP fluorescence of D1-AP_{76} ribozyme upon addition of (saturating) 1000 nM noncleavable substrate analogue (ncS3), cleavable substrate (S3), or 3′-product (3′P), as indicated. The data set for ncS3 was fit with a single-exponential decrease function to yield a rate constant of 1.0 min^{-1} that is reported in panel b. The data set for S3 gave a single-exponential increase that pertains to substrate cleavage with a rate constant of 0.27 min^{-1}. The 3′P data set increases double-exponentially with a fast-phase rate constant of 7.1 min^{-1} (slow phase, 0.1 min^{-1} with 12% of the fast-phase amplitude). In the inset, rescaling of the early data points highlights the slight decrease in AP fluorescence upon formation of the ribozyme−ncS3 complex (○) and the slight lag phase, due to substrate binding, in the fluorescence increase upon cleavage of the S3 substrate (■) (gray line, exponential fit to the increase alone). (b) Concentration dependence of the observed pseudo-first-order rate constant upon addition of excess ncS3 to the ribozyme. The slope of the linear regression line yields the bimolecular binding rate constant k_{on}. (c) Dissociation of the noncleavable substrate analogue from its ribozyme complex. The ribozyme−ncS3 complex (200 nM, with a 1000 nM excess of ncS3) was chased with 4 μM 3′-product, and the resulting increase in 2-aminopurine fluorescence was fit to a single-exponential increase function to yield a dissociation rate constant k_{off} at 0.20 min^{-1} (—). There is no significant dependence on the chase concentration (inset).

Next, we exploited the fact that 3′P has a higher affinity for binding to the HDV ribozyme than the substrate (*4*, *18*), providing an avenue for assessing substrate dissociation. To this end, the ribozyme−ncS3 precursor complex was formed and subsequently chased with a 4 μM excess of 3′P. This resulted in a single-exponential increase in AP_{76} fluorescence due to dissociation of the substrate and replacement with 3′P chase (Figure 3c). The observed rate constant k_{off} of 0.20 min^{-1} is independent of the concentration of chase (inset of Figure 3c). The substrate dissociation and binding rate constants, k_{off} and k_{on}, respectively, measured at 37 °C, define the equilibrium dissociation constant K_D ($=k_{off}/k_{on}$) which equals 110 nM at 37 °C, 3-fold higher than a previously determined value at 25 °C (*18*), as expected for a shift to a higher temperature.

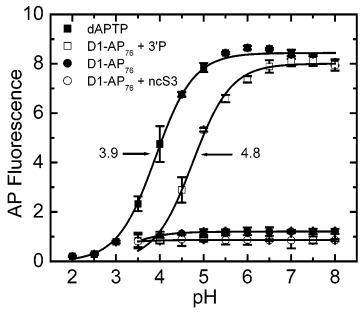

FIGURE 4: Fluorescence of 2-aminopurine 2′-deoxyribose 5′-triphosphate (dAPTP) and 2-aminopurine in position 76 of the D1 ribozyme construct and its complexes as a function of pH (see Materials and Methods). The wavelength of excitation was 290 nm, and the emission spectra were monitored at the AP peak at 360 nm. pK_a values of 3.9 and 4.8 for the free nucleoside triphosphate and the ribozyme−3′P complex, respectively, were derived by fitting the data to the equation $F_{obs} = F_{max}/(1 + 10^{pK_a - pH})$.

The 2-Aminopurine Fluorescence as a Function of pH Reveals Significant Differences in the Chemical Environment of the Catalytic Core before and after Cleavage. Our steady-state AP_{76} fluorescence assays indicate that there are structural differences between the precursor and postcleavage conformations near the catalytic core of the HDV ribozyme. The AP fluorescence in the ribozyme and ribozyme−ncS3 complex is significantly quenched, presumably as a result of local stacking interactions. In contrast, significant unquenching (i.e., unstacking) of AP_{76} is observed upon formation of the 3′-product complex (Figure 3a). On the basis of these observations, we decided to monitor the protonation state of the N1 position of AP_{76} in the ribozyme and its substrate and 3′-product complexes by measuring the fluorescence intensity as a function of pH. At low pH, the relative fluorescence intensity of 2-aminopurine is reduced as a result of N1 protonation (*17*, *35*). First, we measured the pH titration curve of 2-aminopurine 2′-deoxyribose 5′-triphosphate in solution as a control, which resulted in a pK_a of 3.9 (Figure 4), consistent with a previously reported value of 3.8 (*17*). Next, we measured the pH titration curve of the AP_{76} in the ribozyme, the ribozyme−ncS3 complex, and the ribozyme−3′P complex. These curves indicate clear differences in titration of AP_{76} that relate to its local environment (Figure 4). From the pH titration curve of the ribozyme−3′ product complex an AP_{76} pK_a of 4.8 is derived. Although this experimentally determined pK_a is nearly 1 pH unit higher than that of free AP in solution, the AP_{76} fluorescence intensity in this complex essentially titrates as the free base. This result further supports the idea that position 76 in the product complex is looped out and exposed to solvent. Conversely, the fluorescence in the ribozyme and the ribozyme−ncS3 complex is strongly quenched throughout the whole pH range. Although the low intensity of AP_{76} fluorescence in these constructs impedes extraction of reliable pK_as from the titration curves, these curves show that the local environments in the free ribozyme and the ribozyme−

ncS3 complex are very different from that in the ribozyme−3′P complex. These observations are consistent with the notion that significant local structural changes around the catalytic core occur upon cleavage in the HDV ribozyme.

Synchronous 2-Aminopurine Fluorescence and Steady-State FRET Kinetics Suggest that Local and Global Conformational Changes Occur Simultaneously. Previously, we have shown by fluorescence resonance energy transfer (FRET) that this trans-acting HDV ribozyme undergoes a global conformational change upon substrate cleavage (*18*). However, these experiments could not reveal whether this global conformational change is accompanied by local structural rearrangements. In light of our success with AP_{76} as a local conformational probe near the catalytic core of the HDV ribozyme, we sought to test whether the local and global conformational changes are coupled. To this end, we utilized AP_{76} and FRET in concert, by employing a modified strand B of our D1 construct with the $G_{76}AP$ substitution and terminal 5′-fluorescein and 3′-tetramethylrhodamine labels as donor−acceptor FRET pair (Figure 1a). To ensure that all fluorophore-labeled strands are converted into complexes, we added 2- and 5-fold excesses of the unmodified strand A and substrate (or product), respectively (see Materials and Methods). Similar results were obtained when AP_{76} and the FRET fluorophores were incorporated separately into strands B and A, respectively, and used at equimolar concentrations (data not shown).

Figure 5a shows the changes in relative AP_{76} fluorescence and FRET efficiency upon addition of a 1000 nM excess of noncleavable substrate analogue, ncS3, to the assembled AP_{76} and FRET-labeled ribozyme. The synchronous decrease in both signals was fit to single exponentials that yield rate constants of 1.3 and 1.4 min^{-1}, respectively. These values compare well with the rate constant for the AP_{76} fluorescence decrease under identical conditions, but in the absence of the FRET probes (1.0 min^{-1}, Figure 3a).

The AP fluorescence and FRET changes after addition of a saturating concentration of 1000 nM of either cleavable substrate S3 or 3′P to the ribozyme show characteristics expected for formation of the ribozyme−3′-product complex. Specifically, when adding a saturating concentration of S3, we observed an increase in the relative AP fluorescence and a decrease in the relative FRET efficiency (Figure 5b). The two fluorescence changes are again synchronous and, when fit to single-exponential increase and decrease functions, respectively, yield rate constants of 0.21 and 0.24 min^{-1}, respectively. These fluorescence changes are indicative of substrate cleavage and their rate constants comparable to the ones obtained from the radioactive cleavage assay (0.17 min^{-1}) and monitoring of AP_{76} fluorescence in the absence of FRET fluorophores (0.27 min^{-1}).

Finally, when we directly initiated formation of the ribozyme−3′-product complex by adding 3′P to the ribozyme, a substantial increase in the relative AP fluorescence and a synchronous decrease in relative FRET efficiency were observed (Figure 5c), with rate constants of 5.2 and 5.7 min^{-1}, respectively. These values are in reasonable agreement with the value obtained from AP_{76} probing in the absence of FRET probes (7.1 min^{-1}). These results demonstrate that local conformational changes of the trans-acting HDV ribozyme as monitored by AP_{76} fluorescence occur simultaneously with the global conformational changes observed by FRET.

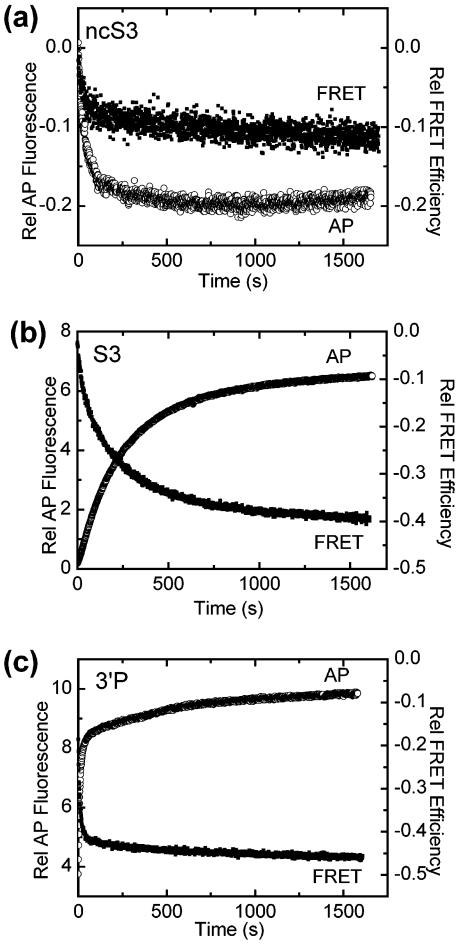

FIGURE 5: Time courses of the relative AP fluorescence (○) and FRET efficiency (■) of the doubly fluorescein- and tetramethylrhodamine-labeled D1-AP_{76} ribozyme upon addition of 1000 nM noncleavable substrate analogue (ncS3), cleavable substrate (S3), or 3′-product (3′P) in 40 mM Tris-HCl (pH 7.5), 11 mM $MgCl_2$, and 25 mM DTT at 37 °C. (a) Formation of the ribozyme−ncS3 complex results in slight decreases in relative AP fluorescence and FRET efficiency with rate constants of 1.3 and 1.4 min^{-1}, respectively. (b) The data sets for S3 pertain to substrate cleavage and give a single-exponential increase in relative AP fluorescence and a concurrent decrease in relative FRET efficiency with rate constants of 0.21 and 0.24 min^{-1}, respectively. (c) Direct formation of the product complex by the addition of 3′P gives a fast double-exponential increase in relative AP fluorescence and a concurrent decrease in FRET efficiency, with fast-phase rate constants of 5.2 and 5.7 min^{-1}, respectively. The slow phases contribute 20 and 11% of their respective fast phases, with rate constants of 0.1 min^{-1} for both the AP fluorescence increase and FRET decrease. In the absence of further studies of their nature, we cannot distinguish whether these phases are due to a small fraction of a second RNA species with slower folding kinetics, or due to a slow second kinetic step in folding of the main RNA species. In either case, the minor slow components do not change our conclusions about the coincidence of local and global folding events as they are present in both the AP and FRET data sets.

A FRET Gel Shift Assay Demonstrates the Homogeneity of the Various, Structurally Distinct Ribozyme Complexes. We utilized a previously described FRET gel mobility assay (*18*) to examine the homogeneity of our various ribozyme complexes. To study the effect that the $G_{76}AP$ substitution has on the overall folding of the ribozyme and its complexes, the doubly labeled $G_{76}AP$ mutant was electrophoresed on a

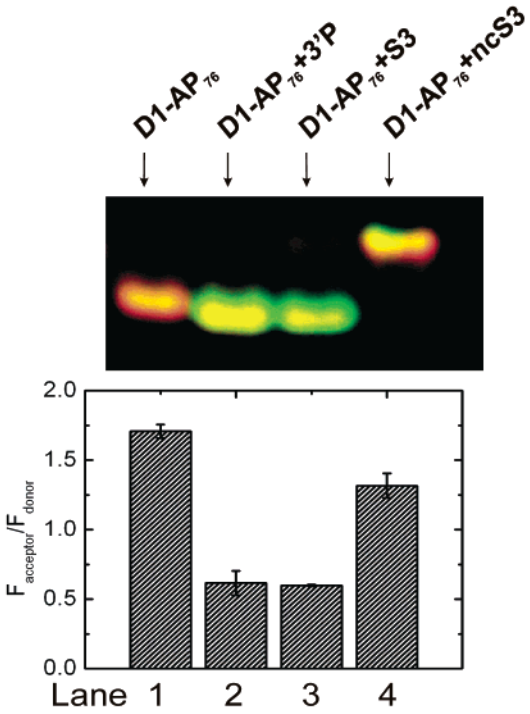

FIGURE 6: Nondenaturing gel electrophoresis of doubly fluorescein- and tetramethylrhodamine-labeled D1-AP_{76} complexes (see Materials and Methods). The free AP_{76} mutant ribozyme (D1-AP_{76}, lane 1) comigrates with its ribozyme−3′-product complex (D1-AP_{76}+3′P, lane 2, top panel), but can be distinguished by the ratio of acceptor to donor fluorescence (bottom panel). The ribozyme−substrate complex (D1-AP_{76}+S3, lane 3) undergoes catalysis and is observed as the ribozyme−3′-product complex. The ribozyme−noncleavable substrate analogue complex (D1-AP_{76}+ncS3, lane 4) stays intact and migrates slower.

nondenaturing polyacrylamide gel alone and in complex with S3, ncS3, and 3′P. The relative FRET efficiencies for all bands in the gel were derived from a quantitative Fluorimager analysis (Figure 6) (see Materials and Methods). We found that the ribozyme alone as well as its complexes migrate as homogeneous populations, with less than 15% of the overall fluorescence intensity resulting from alternate bands (data not shown). The FRET efficiencies of the gel shift bands of the ribozyme and its complexes containing the $G_{76}AP$ substitution are consistent with our steady-state fluorescence assays of this mutant. Lane 1, loaded with ribozyme alone, shows a band with a high FRET ratio ("or red-shifted", i.e., acceptor fluorescence-dominated band). Lane 2, loaded with ribozyme−3′P complex, shows a band that comigrates with the ribozyme alone and has a significantly decreased FRET ratio ("green-shifted"). Lane 3, loaded with the ribozyme−cleavable substrate complex, shows a band that comigrates with the ribozyme−3′P complex, which is the result of substrate cleavage and formation of the ribozyme−3′P complex. Lane 4, loaded with the ribozyme−ncS3 complex, shows a slower migrating band with a slightly decreased FRET ratio (green-shifted). This decrease in FRET efficiency upon formation of the ribozyme D1-AP_{76}−ncS3 complex is consistent with our solution assays (Figure 5a). These findings further support the idea that the precursor conformation is structurally distinct from the postcleavage ribozyme complex.

Time-Resolved FRET Reveals the Global Architectures of the Precursor and Product Complexes. To quantify the global structural changes in the trans-acting $G_{76}AP$ mutant ribozyme upon substrate cleavage, we used time-resolved FRET (tr-FRET) to measure the donor−acceptor distances in the FRET-labeled ribozyme and its substrate and 3′-product complexes as previously described (*18*). To this end, we recorded the time-resolved donor (fluorescein) decay curves of the ribozyme (D1-AP_{76}), ribozyme−noncleavable substrate complex (D1-AP_{76}−ncS3), and ribozyme−3′-product (D1-AP_{76}−3′P) complex, each of them singly labeled with donor as well as doubly labeled with donor and acceptor. The fluorescence decay curves of the donor-only-labeled complexes are nearly identical, and all show mean lifetimes of ~4 ns (data not shown). We have shown previously that the anisotropies of the terminally attached donor and acceptor fluorophores in all HDV ribozyme complexes are low and similar in magnitude (*18*). This suggests that a decrease in donor lifetime in the doubly labeled complex is due to FRET and can be used to calculate donor−acceptor distances. Our tr-FRET data analysis (see Materials and Methods) confirms our results from steady-state FRET in solution and in gels, indicating that there are significant differences in the global architectures, particularly between the ribozyme−substrate and ribozyme−3′-product complexes. In particular, in the free D1-AP_{76} mutant ribozyme, the donor−acceptor distance distribution is centered around a mean distance of 48 Å (full width at half-maximum, fwhm, of 25 Å), in the D1-AP_{76}−ncS3 complex around 52 Å (fwhm of 21 Å), and in the D1-AP_{76}−3′P complex around 65 Å (fwhm of 33 Å) (Table 3). The full width at half-maximum, which is a measure of structural flexibility, suggests that a relatively rigid conformation is acquired prior to cleavage, while the ribozyme−3′-product complex adopts a more flexible conformation upon product formation. Similar results were obtained when the measurements were carried out at 25 °C rather than under standard conditions at 37 °C (data not shown). These results confirm that our preparations are indeed structurally homogeneous, since in all three cases a single distance distribution fits the decay data well, as judged by the residuals and the reduced χ^2 values (<1.2). The tr-FRET data directly support our steady-state fluorescence measurements in that the ribozyme becomes slightly more extended (by 4 Å) when it binds substrate, while it becomes significantly more extended (by 13 Å) upon cleavage and formation of the 3′-product complex.

Table 3: Time-Resolved FRET Analysis of the Doubly Fluorescein- and Tetramethylrhodamine-Labeled D1-AP_{76} Ribozyme and Its Complexes[a]

parameter	D1-AP_{76}	D1-AP_{76}−ncS3	D1-AP_{76}−3′P
mean donor−acceptor distance (Å)	48 ± 1	52 ± 1	65 ± 1
fwhm (Å)	25 ± 1	21 ± 1	33 ± 1
χ^2	1.1	1.2	1.1

[a] Donor−acceptor distances and their full widths at half-maximum (fwhm) were measured as described in Materials and Methods in 40 mM Tris-HCl (pH 7.5), 11 mM $MgCl_2$, and 25 mM DTT at 37 °C; errors were estimated from two independent measurements. χ^2 is the reduced χ^2 value.

DISCUSSION

Biological catalysis depends on the proper positioning of functional groups of an enzyme to increase their "effective

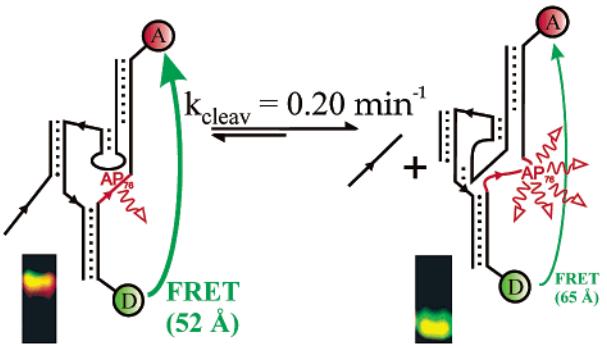

FIGURE 7: Summary of the local and global conformational changes upon trans cleavage by the HDV ribozyme, observed here by 2-aminopurine fluorescence and fluorescence resonance energy transfer (FRET), respectively. 2-Aminopurine in position 76 (AP_{76}) becomes strongly unquenched as a consequence of folding of the trefoil turn in J4/2 (red). At the same time, the distance between a terminal donor (D) and acceptor (A) fluorophore pair increases by ~25%, and we observe a faster migrating, green-shifted FRET gel shift band (bottom).

concentration" and lower the entropic cost of their interaction with the substrate (*31*). RNA catalysts are no exception, as exemplified in the ribozyme from the human hepatitis delta virus. The crystal structure of the self-cleaved product form of the genomic HDV ribozyme (*6*) shows a tightly interwoven nested double-pseudoknot structure with five Watson−Crick base-paired segments (P1, P1.1, P2, P3, and P4) (Figure 1a). In addition, it reveals a trefoil turn in the single-stranded region connecting P4 and P2 (termed J4/2) that pushes the catalytically functional C_{75} within hydrogen bonding distance (~2.7 Å) of the 5′-OH leaving group of the transesterification reaction (Figure 1b). The sequence upstream of the leaving group and including the scissile phosphate (the 5′-product, 5′P; Figure 1a) is absent from the crystal structure, and there is no high-resolution structural information available yet for the reaction precursor (*5*). Our data demonstrate that a trans-acting form of the HDV ribozyme, which allows us to site-specifically incorporate fluorophores as structural probes, undergoes a substantial conformational rearrangement in J4/2 from the precursor to the product complex. In the course of this local rearrangement, the trefoil turn forms and the global conformation changes, as observed by fluorescence resonance energy transfer and summarized in Figure 7.

AP_{76} Reports Formation of the Trefoil Turn in J4/2 upon Cleavage. 2-Aminopurine is a fluorescent guanine analogue that has previously been used to monitor local structural changes in a number of RNAs, including the hammerhead (*23*, *36*) and hairpin ribozymes (*12*, *24*), the HIV Rev responsive element (*37*), aptamers (*38*), hairpins (*39*), and loop−loop kissing complexes (*40*). Its fluorescence is quenched when it stacks on any of the natural nucleobases (*33*, *34*). When AP is incorporated in place of G_{76} of our trans-acting HDV ribozyme construct D1 (Figure 1a), it becomes a probe for rearrangements in local stacking interactions in J4/2. Replacement of G_{76} is particularly appealing since (a) it only modestly perturbs the catalytic activity of the ribozyme (Tables 1 and 2) as expected from previous mutational analyses (*7*) and (b) in the postcleavage crystal structure this nucleotide is unstacked and extrudes into solvent, forming the trefoil turn motif that positions the adjacent C_{75} for general acid (or base) catalysis (Figure 1b). That is exactly what we observe with AP_{76}. Upon formation of the ribozyme−3′-product complex through substrate cleavage or direct 3′P binding, the fluorescence of AP_{76} becomes unquenched (Figure 3a); i.e., the base becomes solvent-exposed. In addition, the fluorescence of AP_{76} strongly increases with pH, like that of the free nucleoside triphosphate, but with an upward shift in pK_a of 0.9 unit (Figure 4), as expected for incorporation of 2-aminopurine into a highly negatively charged RNA (*41*−*43*).

In contrast, the ribozyme−noncleavable substrate analogue (ncS3) complex shows the AP_{76} fluorescence strongly quenched, i.e., the base stacked (Figure 3a), independent of pH (Figure 4). Since AP is quenched by any nucleobase, we cannot derive direct structural information from these data, but it is reasonable to assume that AP_{76} stacks between the adjacent C_{75} and A_{77} (Figure 1a). Without the extrusion of nucleotide 76 into solvent, the trefoil turn of J4/2 with its sharp double reversal in the RNA backbone trajectory cannot form, and presumably, a more regular backbone trajectory will be adopted, as suggested in Figure 1b. As a result, C_{75} will not be within hydrogen bonding distance of the scissile phosphodiester or the phosphate backbone of P1.1 (Figure 1) and cannot be expected to have the strongly shifted pK_a that this cytosine would need to act as a general acid in phosphodiester transfer (*5*, *6*, *9*, *10*). This conclusion is in accord with a recent NMR study that showed that the microscopic pK_a of C_{75} in the precursor of the genomic HDV ribozyme is not shifted toward neutrality (*44*). The same NMR study showed an upward pK_a shift for C_{75} in the product form of only up to 0.6 unit compared to the free nucleoside. This is similar to the 0.9 unit upward shift in pK_a that we observe by pH titration of AP fluorescence for the adjacent AP_{76} in the ribozyme−3′-product complex (Figure 4) and suggests that, electrostatically, the local environments of the two bases are rather similar.

Thus, our data indicate a substantial rearrangement of the catalytic core of the HDV ribozyme along the cleavage reaction trajectory from the precursor to the product form (Figure 7). The trefoil turn in J4/2, as detected by a strongly unquenched AP_{76} fluorescence, is absent from the precursor complex of our trans-acting construct, but clearly formed in the product complex. The unusual pK_a shift of C_{75} as derived from pH profiles of the cleavage kinetics (*8*−*10*, *30*, *45*, *46*) may then relate to a rate-limiting, short-lived pK_a shift in the transition state of the reaction, as proposed previously (*5*, *44*). It is important to note that our FRET gel shift (Figure 6) and time-resolved FRET data (Table 3) suggest that both our precursor and product complexes are structurally homogeneous. In addition, we have independent footprinting data indicating that paired regions P1−P4 are properly formed in both structures, and that P1.1 is formed in the 3′-product complex (S. Jeong and N. G. Walter, unpublished data), as observed in the 3′-product crystal structure (Figures 1a and 7). Rapid structural dynamics which may control access to the transition state, however, will not be resolved by these techniques.

Formation of the Trefoil Turn Coincides with a Previously Observed Change in Global Conformation; Do These Conformational Changes Limit the Overall Reaction Kinetics? Global and local conformational changes in RNA are often coupled. Due to the hierarchical nature of RNA folding [secondary structure forms before tertiary structure (*47*)],

independently folding secondary structures often have to readjust locally (by induced fit) to establish a global tertiary structure. Examples are the hairpin ribozyme (*13*, *24*, *48*, *49*) or the P5abc domain of the *Tetrahymena* group I intron ribozyme (*50*). In previous work, we have shown that the trans-acting HDV ribozyme undergoes a global conformational change upon cleavage, leading to an increase in the distance between the termini of helices P4 and P2 that can be observed as a decrease in the extent of FRET between a donor−acceptor fluorophore pair (*18*). Here, we have expanded this analysis by employing AP fluorescence and FRET in concert and have shown that the formation of the trefoil turn in J4/2 kinetically coincides with the global change in the P4−P2 distance (Figures 5 and 7). Similar measurements on the hairpin ribozyme have demonstrated the kinetic coincidence of local secondary structure readjustments upon formation of long-range tertiary contacts between its domain A and its domain B (*24*). This induced fit involves base flipping of G_{+1} immediately 3′ of the cleavage site in domain A to make a Watson−Crick base pair with C_{25} in domain B, which positions the cleavage site backbone for catalysis (*13*).

In the absence of a high-resolution structure for the precursor of the HDV ribozyme, it is less evident how the local and global conformational changes observed here relate to placement of the scissile phosphate for catalysis. It has been pointed out previously that the 5′-hydroxyl leaving group is deeply buried within the catalytic cleft of the 3′-product crystal structure and that accommodation of a sequence 5′ to the cleavage site may be sterically strenuous (*5*, *18*). Consistent with this notion, Been and co-workers have found that sequence components immediately 5′ to the cleavage site destabilize ground-state binding. This ground-state destabilization appears to contribute up to 2 kcal/mol toward the total 8.5 kcal/mol reduction in activation free energy for RNA cleavage by the HDV ribozyme (*51*). It is therefore tempting to speculate that a bend in the backbone trajectory around the scissile phosphate, the energetic cost of which is dependent on the length and composition of the sequence 5′ to the cleavage site, accompanies formation of the transition state (*5*, *18*). According to this model, the scissile phosphate becomes positioned between the catalytic C_{75} and helices P1 and P1.1 only in this constrained transition state. Hydrogen bonding between C_{75} and a negatively charged scissile phosphate oxygen in the transition state may then explain the apparently transient nature of the pK_a shift of C_{75}, as suggested previously (*11*).

Our capture of significant conformational changes along the reaction trajectory from the precursor to the product forms of the trans-acting HDV ribozyme raises the possibility that these may limit the observed cleavage rate constant. This notion certainly has precedence in other small catalytic RNAs, as cleavage by the hairpin ribozyme is rate-limited by a combination of global conformational transitions and reversible chemistry (*49*), while hammerhead ribozyme activity appears to be limited by a local base flipping event at the cleavage site (*52*). Access to a structurally constrained transition state may also limit the rate of product formation in the trans-acting HDV ribozyme. Our pH profiles in Figure 2b present indirect evidence for this idea; our ∼5-fold slower G_{76}AP mutant has an apparent pK_a that is 0.6 unit lower than that of the G_{76} wild type (5.1 vs 5.7, Table 1). This is consistent with a pH-dependent step being rate-limiting at low pH and a pH-independent conformational change (5-fold slower for the G_{76}AP mutant than for the wild type) becoming rate-determining above pH 5.1 and 5.7, respectively. Interestingly, single-turnover rate constants of all trans-acting HDV ribozymes (0.1−0.9 min^{-1} at 37 °C; see this work as well as refs *4*, *29*, *53*, and *54*) fall into the same range as those for the hairpin (*55*−*57*) and most hammerhead ribozymes (*58*−*60*) which both are rate-limited by conformational changes. In contrast, cleavage in the cis-acting genomic and antigenomic HDV ribozymes is considerably faster with rate constants of ∼8−20 min^{-1} (*5*, *8*, *9*), typically after elaborate preannealing protocols (*30*, *61*). Faster cleavage by the cis-acting ribozymes does not imply that the conformational change observed in the trans-acting ribozymes is absent, but only that it is considerably faster and/or occurs in a fast pre-equilibrium, perhaps due to a higher probability of proper positioning of all functional groups for catalysis. This may be accomplished by the helical crossover at the top of helix P1 that distinguishes cis-acting from most trans-acting HDV ribozymes.

Finally, there is evidence that other local conformational changes in the catalytic core of the HDV ribozyme may occur when it folds into a catalytic structure. For example, an NMR structure of the isolated closing loop of P3 (Figure 1a) revealed a base paring pattern very different from that observed in the 3′-product crystal structure (*62*); formation of P1.1 will be critical to shifting the equilibrium from one base pairing scheme to the other. In fact, a more recent NMR study has found evidence for local conformational changes around many nucleotides in two trans-acting HDV ribozymes (*63*). In addition, differential photo-cross-links to J4/2 and P3 and its closing loop were observed in monovalent versus divalent cations, suggesting a metal ion-dependent conformational change near the cleavage site (*64*). Similarly, the accessibility of the closing loop of P3, as probed by an oligonucleotide hybridization assay, decreased upon addition of magnesium, presumably due to the formation of P1.1 (*65*). Further experimental work will have to clarify whether structural changes in this loop are linked to the local rearrangement of J4/2 upon cleavage as described here.

ACKNOWLEDGMENT

We thank Mary Falgout for help with the fluorescence assays and all members of the Walter group for stimulating discussions, Vladimir Ramirez-Carrozzi and Tom Kerppola for making their FluorImager and expertise on gelFRET assays available to us, and David Millar, Steve Parus, and Steve Katnik for help with setting up our laser-induced time-resolved fluorometer.

REFERENCES

1. Lai, M. M. (1995) *Annu. Rev. Biochem. 64*, 259−286.
2. Hadziyannis, S. J. (1997) *J. Gastroenterol. Hepatol. 12*, 289−298.
3. Macnaughton, T. B., Shi, S. T., Modahl, L. E., and Lai, M. M. (2002) *J. Virol. 76*, 3920−3927.
4. Shih, I., and Been, M. D. (2000) *Biochemistry 39*, 9055−9066.
5. Shih, I. H., and Been, M. D. (2002) *Annu. Rev. Biochem. 71*, 887−917.
6. Ferre-D'Amare, A. R., Zhou, K., and Doudna, J. A. (1998) *Nature 395*, 567−574.

7. Tanner, N. K., Schaff, S., Thill, G., Petit-Koskas, E., Crain-Denoyelle, A. M., and Westhof, E. (1994) *Curr. Biol. 4*, 488−498.
8. Perrotta, A. T., Shih, I., and Been, M. D. (1999) *Science 286*, 123−126.
9. Nakano, S., Chadalavada, D. M., and Bevilacqua, P. C. (2000) *Science 287*, 1493−1497.
10. Oyelere, A. K., Kardon, J. R., and Strobel, S. A. (2002) *Biochemistry 41*, 3667−3675.
11. Nakano, S., Proctor, D. J., and Bevilacqua, P. C. (2001) *Biochemistry 40*, 12022−12038.
12. Pinard, R., Hampel, K. J., Heckman, J. E., Lambert, D., Chan, P. A., Major, F., and Burke, J. M. (2001) *EMBO J. 20*, 6434−6442.
13. Rupert, P. B., and Ferre-D'Amare, A. R. (2001) *Nature 410*, 780−786.
14. Nissen, P., Hansen, J., Ban, N., Moore, P. B., and Steitz, T. A. (2000) *Science 289*, 920−930.
15. Polacek, N., Gaynor, M., Yassin, A., and Mankin, A. S. (2001) *Nature 411*, 498−501.
16. Muth, G. W., Chen, L., Kosek, A. B., and Strobel, S. A. (2001) *RNA 7*, 1403−1415.
17. Ward, D. C., Reich, E., and Stryer, L. (1969) *J. Biol. Chem. 244*, 1228−1237.
18. Pereira, M. J., Harris, D. A., Rueda, D., and Walter, N. G. (2002) *Biochemistry 41*, 730−740.
19. Scaringe, S. A. (2001) *Methods 23*, 206−217.
20. Walter, N. G., and Burke, J. M. (2000) *Methods Enzymol. 317*, 409−440.
21. Walter, N. G., Hampel, K. J., Brown, K. M., and Burke, J. M. (1998) *EMBO J. 17*, 2378−2391.
22. Shih, I. H., and Been, M. D. (1999) *RNA 5*, 1140−1148.
23. Menger, M., Tuschl, T., Eckstein, F., and Porschke, D. (1996) *Biochemistry 35*, 14710−14716.
24. Walter, N. G., Chan, P. A., Hampel, K. J., Millar, D. P., and Burke, J. M. (2001) *Biochemistry 40*, 2580−2587.
25. Walter, N. G., Burke, J. M., and Millar, D. P. (1999) *Nat. Struct. Biol. 6*, 544−549.
26. Walter, N. G. (2001) *Methods 25*, 19−30.
27. Ramirez-Carrozzi, V. R., and Kerppola, T. K. (2001) *Methods 25*, 31−43.
28. Suh, Y. A., Kumar, P. K., Taira, K., and Nishikawa, S. (1993) *Nucleic Acids Res. 21*, 3277−3280.
29. Sakamoto, T., Tanaka, Y., Kuwabara, T., Kim, M. H., Kurihara, Y., Katahira, M., and Uesugi, S. (1997) *J. Biochem. 121*, 1123−1128.
30. Wadkins, T. S., Shih, I., Perrotta, A. T., and Been, M. D. (2001) *J. Mol. Biol. 305*, 1045−1055.
31. Fersht, A. (1999) *Structure and Mechanism in Protein Science*, Freeman, New York.
32. Millar, D. P. (1996) *Curr. Opin. Struct. Biol. 6*, 322−326.
33. Rachofsky, E. L., Osman, R., and Ross, J. B. (2001) *Biochemistry 40*, 946−956.
34. Jean, J. M., and Hall, K. B. (2001) *Proc. Natl. Acad. Sci. U.S.A. 98*, 37−41.
35. Sowers, L. C., Boulard, Y., and Fazakerley, G. V. (2000) *Biochemistry 39*, 7613−7620.
36. Menger, M., Eckstein, F., and Porschke, D. (2000) *Nucleic Acids Res. 28*, 4428−4434.
37. Lacourciere, K. A., Stivers, J. T., and Marino, J. P. (2000) *Biochemistry 39*, 5630−5641.
38. Parrott, A. M., Lago, H., Adams, C. J., Ashcroft, A. E., Stonehouse, N. J., and Stockley, P. G. (2000) *Nucleic Acids Res. 28*, 489−497.
39. Menger, M., Eckstein, F., and Porschke, D. (2000) *Biochemistry 39*, 4500−4507.
40. Rist, M., and Marino, J. (2001) *Nucleic Acids Res. 29*, 2401−2408.
41. Friedrich, K., Woolley, P., and Steinhauser, K. G. (1988) *Eur. J. Biochem. 173*, 233−239.
42. Connell, G. J., and Yarus, M. (1994) *Science 264*, 1137−1141.
43. Legault, P., and Pardi, A. (1994) *J. Magn. Reson., Ser. B 103*, 82−86.
44. Luptak, A., Ferre-D'Amare, A. R., Zhou, K., Zilm, K. W., and Doudna, J. A. (2001) *J. Am. Chem. Soc. 123*, 8447−8452.
45. Shih, I. H., and Been, M. D. (2001) *Proc. Natl. Acad. Sci. U.S.A. 98*, 1489−1494.
46. Nakano, S., and Bevilacqua, P. C. (2001) *J. Am. Chem. Soc. 123*, 11333−11334.
47. Brion, P., and Westhof, E. (1997) *Annu. Rev. Biophys. Biomol. Struct. 26*, 113−137.
48. Hampel, K. J., and Burke, J. M. (2001) *Biochemistry 40*, 3723−3729.
49. Zhuang, X., Kim, H., Pereira, M. J., Babcock, H. P., Walter, N. G., and Chu, S. (2002) *Science 296*, 1473−1476.
50. Wu, M., and Tinoco, I., Jr. (1998) *Proc. Natl. Acad. Sci. U.S.A. 95*, 11555−11560.
51. Shih, I., and Been, M. D. (2001) *EMBO J. 20*, 4884−4891.
52. Murray, J. B., Dunham, C. M., and Scott, W. G. (2002) *J. Mol. Biol. 315*, 121−130.
53. Been, M. D., and Wickham, G. S. (1997) *Eur. J. Biochem. 247*, 741−753.
54. Deschenes, P., Lafontaine, D. A., Charland, S., and Perreault, J. P. (2000) *Antisense Nucleic Acid Drug Dev. 10*, 53−61.
55. Esteban, J. A., Banerjee, A. R., and Burke, J. M. (1997) *J. Biol. Chem. 272*, 13629−13639.
56. Shippy, R., Siwkowski, A., and Hampel, A. (1998) *Biochemistry 37*, 564−570.
57. Fedor, M. J. (2000) *J. Mol. Biol. 297*, 269−291.
58. Fedor, M. J., and Uhlenbeck, O. C. (1992) *Biochemistry 31*, 12042−12054.
59. Baidya, N., and Uhlenbeck, O. C. (1997) *Biochemistry 36*, 1108−1114.
60. Stage-Zimmermann, T. K., and Uhlenbeck, O. C. (1998) *RNA 4*, 875−889.
61. Chadalavada, D. M., Senchak, S. E., and Bevilacqua, P. C. (2002) *J. Mol. Biol. 317*, 559−575.
62. Lynch, S. R., and Tinoco, I., Jr. (1998) *Nucleic Acids Res. 26*, 980−987.
63. Tanaka, Y., Tagaya, M., Hori, T., Sakamoto, T., Kurihara, Y., Katahira, M., and Uesugi, S. (2002) *Genes Cells 7*, 567−579.
64. Rosenstein, S. P., and Been, M. D. (1996) *Biochemistry 35*, 11403−11413.
65. Ananvoranich, S., and Perreault, J. P. (2000) *Biochem. Biophys. Res. Commun. 270*, 600−607.
66. Leontis, N. B., and Westhof, E. (2001) *RNA 7*, 499−512.

BI026101M